A Convex Quasistatic Time-stepping Scheme for Rigid Multibody Systems with Contact and Friction

A Convex Quasistatic Time-stepping Scheme for Rigid Multibody Systems with Contact and Friction

Tao Pang and Russ Tedrake
{*pangtao*, *russt*}@csail.mit.edu

***Abstract*— Motion planning for robotic manipulation makes heavy use of quasistatic models, but these same models have not yet proven useful for simulation. This is because in many multi-contact situations, the quasistatic models do not describe a unique next state for the system. A planner is able to use these models optimistically (checking only for feasibility of a motion), but simulation requires more.**

In this work, we enable quasistatic models to uniquely determine contact forces by modeling actuated robots as impedances instead of prescribed motions. Using this model with a well-known convex relaxation for Coulomb friction, time-stepping of quasistatic models can be formulated as a convex Quadratic Program (QP). This convex relaxation does admit mild non-physical behavior between relatively-sliding objects, but through simulations of various complexity, we show that the proposed quasistatic time-stepping scheme generates mostly physically-realistic behaviors, and scales well with the complexity of the simulated systems.

I. Introduction

Robot manipulators interact with the environment and accomplish tasks exclusively through making and breaking frictional contact. It remains challenging to automatically synthesize, from first principles, plans and controllers for contact-rich tasks. An import aspect of tackling this challenge is a physics model that is both accurate and computationally simple, but faster computation almost invariably comes at the cost of less physical realism.

Multibody dynamics with contact and friction is commonly formulated as Linear Complementarity Problems (LCP) [1], [2], which has worst-case NP-hard complexity in the number contacts [3]. As a result, there have been a number of computationally superior convex relaxations of the Coulomb friction constraints [4]–[6]. Although a certain degree of physical realism is sacrificed in exchange for convexity, these convex formulations are sufficiently realistic and have been widely adopted in robotics research [7].

Another avenue to simplify multibody dynamics is to assume that the system is quasistatic, which means velocities of the bodies in the system are sufficiently small so that Coriolis forces and accelerations can be ignored. Therefore, instead of satisfying Newton's second law, bodies in a quasistatic system are always in force equilibrium. Compared with its second-order counterpart, a quasistatic system has half as many states, and its integration can circumvent the computation of terms required by second-order dynamics, such as the mass matrix.

The simplicity of quasistatic models has long been capitalized in the planning of manipulation tasks, such as planar pushing [8]–[11] and grasping [12], [13]. However, existing quasistatic planners only search for a sequence of robot motion and contact forces that satisfy force balance, but neglect to ensure that the planned forces can be uniquely generated by the motion. This problem does not manifest in simple tasks such as planar pushing, where motion does uniquely determine force. On the other hand, it can be crippling in more complex tasks such as grasping: contact forces between the gripper and the object are ambiguous when non-penetration constraints are active, which means the gripper can be merely grazing the object but not grasping it. Efforts have been made to make the contact forces unique [14], [15]. However, the approach in [14] is too computationally expensive; and the approach in [15] applies only to planar objects supported on a tabletop.

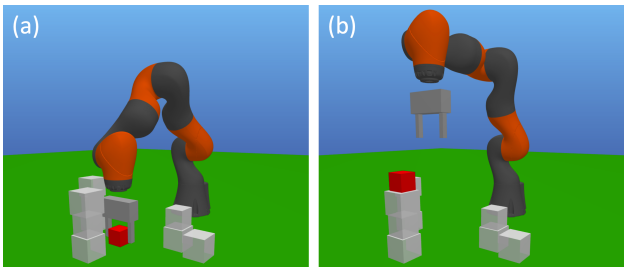

Fig. 1: KUKA IIWA robot stacking cubes. The red cube starts off on the ground (**a**) and is placed on a stack of cubes (**b**).

In this work, we propose a convex time-stepping scheme suitable for predicting the motion and forces of a quasistatic system in response to robot position commands in general 3D manipulation settings, e.g. Fig. 1. By modeling actuators as impedances, commanded and actual robot joint positions are allowed to be different, and the difference uniquely determines contact forces. Using Anitescu's convex relaxation of Coulomb's friction law [4], the quasistatic dynamics with contact and friction of both the actuated robot and the passive objects can be formulated as the Karush–Kuhn–Tucker (KKT) optimality condition of a convex QP. Leveraging powerful commercial QP solvers, the proposed time-stepping scheme scales well with the number of degrees of freedom (DOF) and the number of contacts.

II. Related work

A. LCP and its convex alternatives

In the standard LCP formulation of rigid body dynamics with frictional contact [1], [2], complementarity constraints are utilized to ensure that (**i**) an object cannot apply a force on another object if they are not in contact, and that (**ii**) the contact force satisfies the Coulomb friction law. Without

This work is supported by Amazon and Lincoln Lab/Air Force Award PO# 7000470769.

friction, second-order dynamics with frictionless unilateral contacts can be written as the KKT condition of a convex QP [16]. However, the standard Coulomb friction law introduces non-convex constraints, making the resulting problem more computationally challenging.

In the popular MuJoCo simulator [5], rigid body dynamics with frictional contact is formulated as a convex QP which minimizes the system's kinetic energy subject to friction cone constraints. Regularizing terms are added to the objective function to speed up computation and make the dynamics invertible. MuJoCo can simulate common robotic systems orders of magnitude faster than real time, but a side effect of the additional non-physical terms is "contact force at a distance": contact forces between two bodies can be non-zero even before they make contact [17].

By expressing a friction force as the sum of its components along the extreme rays of a polyhedral approximation of the friction cone, Anitescu provides an alternative formulation of the Coulomb friction constraints that can be expressed as the KKT condition of a convex QP [4]. Anitescu's friction constraints exactly reproduce Coulomb friction when the contact is sticking, while injecting mild non-physical behavior when sliding. Moreover, although originally derived for second-order systems, Anitescu's friction constraints can be easily integrated with quasistatic dynamics to produce a time-stepping scheme for quasistatic systems, which we will show in Section IV.

B. Quasistatic systems in robotic manipulation

The quasistatic assumption has a long history in the planning of planar pushing tasks. Pioneering work by Mason and Lynch focuses on predicting the motion of an object supported on a horizontal surface without knowledge of the pressure distribution between the object and the surface [8], [9]. Later work incorporates a detailed pressure distribution [18], [19] and stochasticity [11] into the quasistatic planar pushing model. Such models have been effectively employed in a Model Predictive Control (MPC) framework which enables an object pushed by a single point contact to track complex planar trajectories [10].

Quasistatic models have also been adopted in dexterous manipulation planning. In [12], joint angle trajectories of a 2D dexterous hand, which transform a grasped workpiece from one grasp configuration to another, are computed using a quasistatic model. The LCP used for grasp planning is detailed in [13], which has several insightful ideas we have borrowed.

As for simulation schemes based on quasistatic models, the earliest work we have found is by Trinkle *et al.* [20], which assumes robot position commands can be perfectly executed, and hence suffers from the same limitations as the traditional quasistatic models used in planning. To address these limitations, in previous work we leveraged the common technique of modeling compliance at the contact points [21] to make the contact forces unique. In addition, the robot's actual positions are allowed to be different from the commanded positions, with the difference minimized in the objective of a Mixed-Integer Quadratic Program (MIQP) [14]. Although this scheme applies to 3D multibody systems, the complexity of MIQP scales exponentially with the number of contacts. On the other hand, the issues with traditional quasistatic models can also be overcome by explicitly modeling the velocity controller, which exerts torques on the robot when the commanded and actual joint velocities are different [15]. While the formulation remains an LCP, it is developed specifically for planar systems where contact can be modeled using limit surfaces [18].

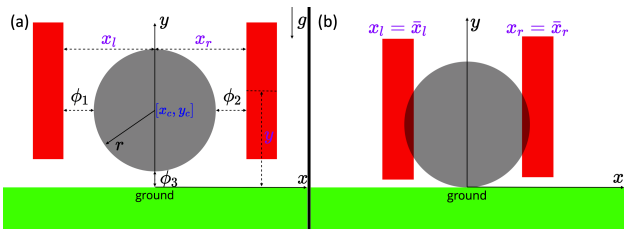

Fig. 2: (**a**) A planar quasistatic multibody system. The red rectangles are the actuated gripper fingers, $\boldsymbol{q}_a = [x_l, x_r, y]$. The gray sphere is the un-actuated manipuland, $\boldsymbol{q}_u = [x_c, y_c]$. $r = 0.1\text{m}$. (**b**) A grasping command violating the non-penetration constraint.

III. LCP FORMULATION FOR QUASISTATIC MULTIBODY SYSTEMS WITH CONTACT

A. Defining quasistatic systems

A generic discrete-time dynamical system is written as $\boldsymbol{x}^{l+1} = \boldsymbol{f}\left(\boldsymbol{x}^l, \boldsymbol{u}^l\right)$, where $\boldsymbol{x}$ is the state and $\boldsymbol{u}$ the input. For second-order rigid multibody systems, $\boldsymbol{x} = [\boldsymbol{q}^\intercal, \boldsymbol{v}^\intercal]^\intercal$ and the input $\boldsymbol{u}$ consists of the generalized forces. In contrast, it is more convenient to think of quasistatic systems as being "driven forward" by the position command of the robot's actuators, rather than by forces [13].

More formally, we can partition the configuration $\boldsymbol{q}$ into two parts: $\boldsymbol{q} = [\boldsymbol{q}_u^\intercal, \boldsymbol{q}_a^\intercal]^\intercal$, where $\boldsymbol{q}_u \in \mathbb{R}^{n_u}$ is the un-actuated (passive) DOFs and $\boldsymbol{q}_a \in \mathbb{R}^{n_a}$ the actuated (actively-controlled) DOFs. The state of a quasistatic system consists of the configuration $\boldsymbol{q}$ only, and the input $\boldsymbol{u}$ is chosen as the *commanded* actuated DOFs, denoted by $\bar{\boldsymbol{q}}_a$.

An example of a quasistatic system in a robotic manipulation setting is shown in Fig. 2a. The system has three actuated DOFs: x_l and x_r are the translation of the left and right gripper fingers along the x-axis, respectively; y is the translation of both fingers along the y-axis. The two un-actuated DOFs, x_c and y_c, are the x and y translation of the sphere.

B. Quasistatic LCP formulation for planning

In this section, we introduce the notations to be used in the rest of the paper, and summarize the quasistatic LCP formulation formalized in [20], which has been traditionally used in manipulation planning.

For a multibody system, let n_c denote the number of contacts, $\boldsymbol{q} \in \mathbb{R}^{n_q}$ the generalized coordinates and $\boldsymbol{v} \in \mathbb{R}^{n_v}$ the generalized velocities. The Jacobian of the contact pair indexed by i is written as $\boldsymbol{J}_{c_i} = \frac{\partial \mathbf{v}_i}{\partial \boldsymbol{v}} \in \mathbb{R}^{3 \times n_v}$, where $\mathbf{v}_i \in \mathbb{R}^3$ is the relative Cartesian velocity between the two bodies of the contact pair. Details of computing $\boldsymbol{J}_{c_i}$ can be found in Section III-b of [14].

For contact i, let $\mathbf{n}_i \in \mathbb{R}^3$ be the Cartesian contact normal and $\mathbf{D}_i = [\mathbf{d}_{i1}, \ldots, \mathbf{d}_{in_d}] \in \mathbb{R}^{3\times n_d}$ a balanced set of n_d Cartesian tangent vectors. The corresponding normal and tangent vectors in generalized coordinates is written as $\boldsymbol{n}_i = (\boldsymbol{J}_{c_i})^\mathsf{T} \mathbf{n}_i \in \mathbb{R}^{n_v}$ and $\boldsymbol{D}_i = [\boldsymbol{d}_{i1}, \ldots, \boldsymbol{d}_{in_d}] = (\boldsymbol{J}_{c_i})^\mathsf{T} \mathbf{D}_i \in \mathbb{R}^{n_v \times n_d}$. We also define $\boldsymbol{N} = [\boldsymbol{n}_1, \ldots, \boldsymbol{n}_{n_c}]$ and $\boldsymbol{D} = [\boldsymbol{D}_1, \ldots, \boldsymbol{D}_{n_c}]$, which stack the normal and tangent vectors from all contacts.

We use $\boldsymbol{\lambda}_n^{l+1} = [\boldsymbol{\lambda}_{n_1}^{l+1}, \ldots, \boldsymbol{\lambda}_{n_{n_c}}^{l+1}] \in \mathbb{R}^{n_c}$ to represent the impulse of normal components of contact forces over the time interval $t \in (lh, (l+1)h]$, where h is the step size of the discretized dynamics. Analogously, for contact i, let $\boldsymbol{\lambda}_{f_i}^{l+1} \in \mathbb{R}^{n_d}$ denote the impulses of the projection of the contact force along the tangent vectors $\boldsymbol{D}_i^l$. The tangential impulses from all contacts can then be written as $\boldsymbol{\lambda}_f^{l+1} = \left[\left(\boldsymbol{\lambda}_{f_1}^{l+1}\right)^\mathsf{T}, \ldots, \left(\boldsymbol{\lambda}_{f_{n_c}}^{l+1}\right)^\mathsf{T}\right]^\mathsf{T} \in \mathbb{R}^{n_c \times n_d}$.

Using the notations introduced above, the standard quasistatic LCP formulation can be written as

$$\text{Find } \boldsymbol{v}^{l+1}, \boldsymbol{\lambda}_n^{l+1}, \boldsymbol{\lambda}_f^{l+1}, \boldsymbol{\Gamma}^l, \text{ subject to} \tag{1a}$$

$$h\boldsymbol{v}_a^{l+1} = \bar{\boldsymbol{q}}_a^{l+1} - \boldsymbol{q}_a^l, \tag{1b}$$

$$\mathbf{0} = \boldsymbol{N}^l \boldsymbol{\lambda}_n^{l+1} + \boldsymbol{D}^l \boldsymbol{\lambda}_f^{l+1} + h\boldsymbol{\tau}^l, \tag{1c}$$

$$\mathbf{0} \le \boldsymbol{\lambda}_{n_i}^{l+1} \perp \phi_i^l + h\left(\boldsymbol{n}_i^l\right)^\mathsf{T} \boldsymbol{v}^{l+1} \ge \mathbf{0}, \forall i \in \mathcal{A}(\boldsymbol{q}^l, \epsilon), \tag{1d}$$

$$\mathbf{0} \le \boldsymbol{\lambda}_f^{l+1} \perp \Gamma_i^l \boldsymbol{e}_i + h\left(\boldsymbol{D}_i^l\right)^\mathsf{T} \boldsymbol{v}^{l+1} \ge \mathbf{0}, \forall i \in \mathcal{A}(\boldsymbol{q}^l, \epsilon), \tag{1e}$$

$$0 \le \Gamma_i^l \perp \mu_i \boldsymbol{\lambda}_{n_i}^{l+1} - \boldsymbol{e}_i^\mathsf{T} \boldsymbol{\lambda}_{f_i}^{l+1} \ge 0, \forall i \in \mathcal{A}(\boldsymbol{q}^l, \epsilon). \tag{1f}$$

where $\boldsymbol{a} \perp \boldsymbol{b}$ for vectors $\boldsymbol{a}$ and $\boldsymbol{b}$ means that $\boldsymbol{a}^\mathsf{T}\boldsymbol{b} = 0$; the superscript l in each term denotes the time step at which the term is evaluated; ϕ_i^l is the signed distance at contact i; $\boldsymbol{\tau}$ collects non-contact external generalized forces acting on the system, including gravity; $\boldsymbol{e}_i$ is a vector of ones; μ_i is the friction coefficient of contact i; $\boldsymbol{\Gamma}^l = [\Gamma_1, \ldots, \Gamma_{n_c}] \in \mathbb{R}^{n_c}$ are slack variables; and $\mathcal{A}(\boldsymbol{q}^l, \epsilon)$ is the index set of contact pairs whose signed distance at time step l is less than a user-defined threshold ϵ, $|\mathcal{A}(\boldsymbol{q}^l, \epsilon)| = n_c$. If $\epsilon = \infty$, n_c is equal to the number of all collision pairs in the system. In practice, ϵ is set to a smaller number to speed up collision queries, and n_c can vary across time steps.

Constraint (1b) states that the position command $\bar{\boldsymbol{q}}_a^{l+1}$ is perfectly executed. (1c) is the force balance condition characteristic of quasistatic systems. (1d) ensures there is no penetration between rigid bodies. Coulomb friction law, including friction cone and maximum dissipation, is enforced by (1e) and (1f).

After solving (1) for $\boldsymbol{v}^{l+1}$, the configuration at the next time step, $\boldsymbol{q}^{l+1}$, can be obtained from

$$\begin{bmatrix} \boldsymbol{q}_u^{l+1} \\ \boldsymbol{q}_a^{l+1} \end{bmatrix} = \begin{bmatrix} \boldsymbol{q}_u^l \\ \boldsymbol{q}_a^l \end{bmatrix} + h \begin{bmatrix} \boldsymbol{G}(\boldsymbol{q}^l) & \mathbf{0} \\ \mathbf{0} & \boldsymbol{I} \end{bmatrix} \begin{bmatrix} \boldsymbol{v}_u^{l+1} \\ \boldsymbol{v}_a^{l+1} \end{bmatrix}, \tag{2}$$

where we assume that the robot has a fixed base and is fully-actuated. On the other hand, the linear transformation $\boldsymbol{G}$ may not be identity, for example, when rotation of floating-based objects is parameterized by quaternions.

Although consistent with intuition, formulation (1) is an ill-posed dynamical system: (**i**) it is possible to command a $\bar{\boldsymbol{q}}_a$ that makes the non-penetration constraint (1d) infeasible; (**ii**) when two bodies are in contact, the contact force between them can be undetermined [14], [15]. Instead of belonging to a niche set of contrived corner cases, such issues arise naturally and frequently in even the simplest robotic manipulation tasks. Consider the example in Fig. 2a, where the fingers are commanded to grasp the sphere. For PD-controlled grippers, it is common to command a small amount of penetration to establish contact forces. However, such commands would violate the non-penetration constraint (1d), as shown in Fig. 2b. On the other hand, even if the fingers are commanded to "graze" the sphere ($\phi_1 = \phi_2 = 0$), which keeps (1d) feasible, any non-negative contact force $\boldsymbol{\lambda}_{n_1}$ and $\boldsymbol{\lambda}_{n_2}$ would satisfy (1c)-(1f). This is problematic if the fingers are also commanded to move up: small contact forces would leave the sphere on the ground, but large contact forces would generate enough friction to lift up the sphere. This model simply cannot determine whether the sphere moves with the hand or stays on the table.

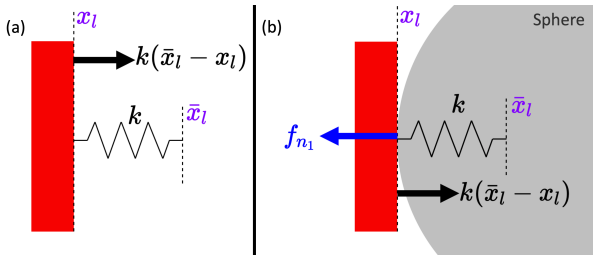

Fig. 3: Free-body diagrams of the left finger when it is (**a**) away from the sphere, and (**b**) in contact with the sphere.

C. Quasistatic LCP formulation with actuators modeled as impedances

The ill-posedness of (1) can be resolved by connecting $\boldsymbol{q}_a$ and $\bar{\boldsymbol{q}}_a$ with springs of 0 rest lengths. To illustrate how the spring helps, we focus on x_l, the prismatic joint of left finger in the planar grasping example in Fig. 2a. Force balance for x_l is given by

$$k(\bar{x}_l - x_l) + f_{n_1} = 0, \tag{3}$$

where k is the stiffness of the spring, $k(\bar{x}_l - x_l)$ is the spring force acting on the left finger, and f_{n_1} the force from contact with the sphere.

When the left finger is not in the vicinity of the sphere (Fig. 3a), we have $f_{n_1} = 0$, which together with (3) implies that $x_l = \bar{x}_l$. Therefore, in the absence of contact, adding the spring has the same effect as (1b). On the other hand, when the left finger is commanded to squeeze the sphere (Fig. 3b), x_l and $\bar{x}_l$ are different due to the non-penetration constraint. The spring force $k(x_l - \bar{x}_l)$ is balanced by the contact force f_{n_1}.

The addition of the spring resolves both issues with (1): (**i**) feasibility of the non-penetration constraint is retained by allowing x_l to be different from its commanded value $\bar{x}_l$; (**ii**) the magnitude of the contact force is also uniquely determined by the difference between x_l and $\bar{x}_l$.

Although adding springs between $\boldsymbol{q}_a$ and $\bar{\boldsymbol{q}}_a$ may seem arbitrary, it is equivalent to modeling the actuators as impedances [22]. For instance, the closed-loop dynamics of

the KUKA IIWA arm in joint-impedance mode is:

$$\boldsymbol{M}(\boldsymbol{q})\ddot{\boldsymbol{q}} + \left(\boldsymbol{D}_{\boldsymbol{q}} + \boldsymbol{C}(\boldsymbol{q}, \dot{\boldsymbol{q}})\right)\dot{\boldsymbol{q}} + \boldsymbol{K}_{\boldsymbol{q}}\left(\boldsymbol{q} - \bar{\boldsymbol{q}}\right) = \boldsymbol{\tau}_{\text{ext}}, \quad (4)$$

where $\boldsymbol{q}$ is the joint angles, $\boldsymbol{M}(\boldsymbol{q})$ the mass matrix, $\boldsymbol{C}(\boldsymbol{q}, \dot{\boldsymbol{q}})$ the Coriolis force, $\boldsymbol{K}_{\boldsymbol{q}}$ the diagonal joint stiffness matrix, $\boldsymbol{D}_{\boldsymbol{q}}$ the diagonal damping matrix and $\boldsymbol{\tau}_{\text{ext}}$ the joint torque generated by external contact [23]. Discarding terms related to velocity and acceleration, the second-order dynamics (4) becomes

$$\boldsymbol{K}_{\boldsymbol{q}}\left(\boldsymbol{q} - \bar{\boldsymbol{q}}\right) = \boldsymbol{\tau}_{\text{ext}}, \quad (5)$$

which can be interpreted as the joint space version of (3).

In summary, the LCP formulation for quasistatic systems with actuators modeled as impedances can be written as

$$\text{Find } \boldsymbol{v}^{l+1}, \boldsymbol{\lambda}_n^{l+1}, \boldsymbol{\lambda}_f^{l+1}, \boldsymbol{\Gamma}^l, \text{ subject to} \quad (6a)$$

$$\boldsymbol{0} = \boldsymbol{N}_u^l \boldsymbol{\lambda}_n^{l+1} + \boldsymbol{D}_u^l \boldsymbol{\lambda}_f^{l+1} + h\boldsymbol{\tau}_u, \quad (6b)$$

$$\boldsymbol{0} = \boldsymbol{N}_a^l \boldsymbol{\lambda}_n^{l+1} + \boldsymbol{D}_a^l \boldsymbol{\lambda}_f^{l+1} + h\boldsymbol{\tau}_a + h\boldsymbol{K}_{\boldsymbol{q}_a}\left(\Delta\bar{\boldsymbol{q}}_a^l - h\boldsymbol{v}_a^{l+1}\right) \quad (6c)$$

$$\text{(1d), (1e) and (1f),} \quad (6d)$$

where $\Delta\bar{\boldsymbol{q}}_a^l = \bar{\boldsymbol{q}}_a^{l+1} - \boldsymbol{q}_a^l$; the subscripts u or a in $\boldsymbol{N}^l$ and $\boldsymbol{D}^l$ indicates sub-matrices formed by the rows of the original matrix corresponding to the un-actuated or actuated DOFs, i.e. $\boldsymbol{N}_u^l \in \mathbb{R}^{n_u \times n_c}$ and $\boldsymbol{D}_a^l \in \mathbb{R}^{n_a \times n_d}$; $\boldsymbol{K}_{\boldsymbol{q}_a}$ is the diagonal stiffness matrix of the actuators' impedance controllers. Except for the separate force balance conditions for impedance-controlled actuators (6b) and un-actuated objects (6c), formulation (6) is identical to (1).

IV. Quasistatic Time-stepping as QP

A. Anitescu's friction constraints

For a generic 3D contact indexed by i with n_{d_i} balanced vectors spanning the contact tangent plane, Anitescu's friction constraints [4] consist of n_{d_i} complementarity constraints:

$$0 \le \beta_{ij} \perp \boldsymbol{n}_i^\intercal \boldsymbol{v} + \mu_i \boldsymbol{d}_{ij}^\intercal \boldsymbol{v} + \phi_i/h \ge 0, \ \forall j = 1, \ldots, n_{d_i}. \quad (7)$$

where β_{i1} and β_{i2} are the components of the contact force along the extreme rays of the friction cone.

In this section, instead of focusing on mathematical properties such as convergence and boundedness, which are already discussed thoroughly in [4], we will try to give some intuition about how the constraints operate in different contact modes. For simplicity, we limit our discussion to 2D, noting that behaviors in 2D generalize easily to 3D.

Specializing (7) to 2D with $n_{d_i} = 2$ gives

$$0 \le \beta_{i1} \perp v_{n_i} + \mu_i v_{d_i} + \phi_i/h \ge 0, \quad (8a)$$

$$0 \le \beta_{i2} \perp v_{n_i} - \mu_i v_{d_i} + \phi_i/h \ge 0, \quad (8b)$$

where $v_{n_i} = \boldsymbol{n}_i^\intercal \boldsymbol{v}$ is the normal component of the relative contact velocity $\mathbf{v}_i$, and $v_{d_i} = \boldsymbol{d}_{i1}^\intercal \boldsymbol{v} = -\boldsymbol{d}_{i2}^\intercal \boldsymbol{v}$ the tangential component. These quantities are illustrated in Fig. 4.

Note that (**i**) the feasible region of $\mathbf{v}_i$ comes from the RHS of (8a) and (8b); (**ii**) both boundaries of the feasible region of $\mathbf{v}_i$ (the blue and red dashed lines in Fig. 4) intersect the $\mathbf{n}_i$-axis at $-\phi_i/h$, which is non-positive; (**iii**) the normal and tangential contact force impulses are given respectively by $\lambda_{n_i} = \beta_{i1} + \beta_{i2}$ and $\lambda_{f_{i1}} = \mu_i\left(\beta_{i1} - \beta_{i2}\right)$.

1) Rolling (Fig. 4a): In a rolling contact, $\mathbf{v}_i = \mathbf{0}$, $\phi_i = 0$ and the contact force is inside the friction cone. The conditions $\mathbf{v} = \mathbf{0}$ and $\phi_i = 0$ imply that $v_{n_i} + \mu_i v_{d_i} + \phi_i/h = 0$ and $v_{n_i} - \mu_i v_{d_i} + \phi_i/h = 0$, i.e. the RHS of (8a) and (8b) are active. Therefore, both β_{1i} and β_{1i} can be positive, allowing any contact force inside the friction cone. In this case, Anitescu's constraints are identical to Coulomb's friction law.

2) Sliding (Fig. 4b) : In a sliding contact, the contact force is on the boundary of the friction cone, and the relative velocity $\mathbf{v}_i$ is horizontal and opposing the friction force. Without loss of generality, we can assume $\beta_{i2} > 0$ and $\beta_{i1} = 0$. Hence the RHS of (8b) is active, i.e. $\mathbf{v}_i$ is constrained to the red dashed line defined by $v_{n_i} - \mu_i v_{d_i} + \phi_i/h = 0$. As $\mathbf{v}_i$ is also horizontal and non-zero per the definition of sliding, the intersection of the red dashed line with the $\mathbf{d}$-axis must be positive, which indicates that $\phi_i > 0$. This is the source of the non-physical behavior of Anitescu's friction constraints: when one body is sliding relative to the other, the body slides in a "boundary layer" of the other body instead of on its surface.

3) Separation (Fig. 4c): Separation indicates that there is no contact force, i.e. $\beta_{1i} = \beta_{2i} = 0$. Hence $\mathbf{v}_i$ can take any value in the feasible region defined by the RHS of (8a) and (8b). For moderate μ_i and reasonably large ϕ_i, the feasible region is large enough to accommodate a wide range of velocities.

B. Putting everything together

We can now combine Anitescu's friction constraints (7) with (6b)-(6c), the force balance constraints with impedance-controlled actuators, yielding the following LCP:

$$\text{Find } \boldsymbol{v}^{l+1}, \text{ subject to}$$

$$\sum_{i \in \mathcal{A}(\boldsymbol{q}^l, \epsilon)} \sum_{j=1}^{n_{d_i}} \left[\boldsymbol{n}_{i,u}^l + \mu_i \boldsymbol{d}_{ij,u}^l\right] \beta_{ij} + h\boldsymbol{\tau}_u = \boldsymbol{0}, \quad (9a)$$

$$\sum_{i \in \mathcal{A}(\boldsymbol{q}^l, \epsilon)} \sum_{j=1}^{n_{d_i}} \left[\boldsymbol{n}_{i,a}^l + \mu_i \boldsymbol{d}_{ij,a}^l\right] \beta_{ij} + h\boldsymbol{\tau}_a + h\boldsymbol{K}_{\boldsymbol{q}_a}\left(\Delta\bar{\boldsymbol{q}}_a^l - h\boldsymbol{v}_a^{l+1}\right) = \boldsymbol{0}, \quad (9b)$$

$$0 \le \phi_i^l + h\left(\begin{bmatrix}\boldsymbol{n}_{i,u}^l \\ \boldsymbol{n}_{i,a}^l\end{bmatrix} + \mu_i \begin{bmatrix}\boldsymbol{d}_{ij,u}^l \\ \boldsymbol{d}_{ij,a}^l\end{bmatrix}\right)^\intercal \begin{bmatrix}\boldsymbol{v}_u^{l+1} \\ \boldsymbol{v}_a^{l+1}\end{bmatrix} \perp \beta_{ij} \ge 0 \quad \forall i \in \mathcal{A}(\boldsymbol{q}^l, \epsilon), j \in \{1 \ldots n_d\}, \quad (9c)$$

where in (9a) and (9b), the contact force is expressed as the sum of the components along the friction cone's extreme rays, instead of the normal and tangential components as in (6b)-(6c).

As pointed out in [4], the LCP (9) can be expressed as the KKT condition of the following QP:

$$\min_{\boldsymbol{v}^{l+1}} \frac{h^2}{2}\left(\boldsymbol{v}_a^{l+1}\right)^\intercal \boldsymbol{K}_{\boldsymbol{q}_a} \boldsymbol{v}_a^{l+1} - h\begin{bmatrix}\boldsymbol{\tau}_u \\ \boldsymbol{K}_{\boldsymbol{q}_a}\Delta\bar{\boldsymbol{q}}_a^l + \boldsymbol{\tau}_a\end{bmatrix}^\intercal \begin{bmatrix}\boldsymbol{v}_u^{l+1} \\ \boldsymbol{v}_a^{l+1}\end{bmatrix} \quad \text{subject to} \quad (10a)$$

$$\frac{\phi_i^l}{h} + \left(\begin{bmatrix}\boldsymbol{n}_{i,u}^l \\ \boldsymbol{n}_{i,a}^l\end{bmatrix} + \mu_i \begin{bmatrix}\boldsymbol{d}_{ij,u}^l \\ \boldsymbol{d}_{ij,a}^l\end{bmatrix}\right)^\intercal \begin{bmatrix}\boldsymbol{v}_u^{l+1} \\ \boldsymbol{v}_a^{l+1}\end{bmatrix} \ge 0 \quad \forall i \in \mathcal{A}(\boldsymbol{q}^l, \epsilon), j \in \{1 \ldots n_d\}. \quad (10b)$$

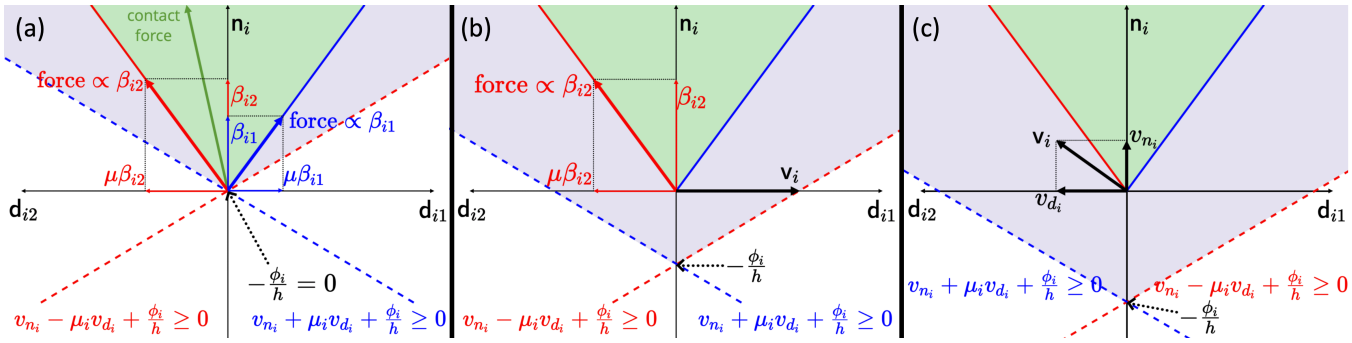

Fig. 4: Contact modes of Anitescu's friction constraints (8): (**a**) sticking, (**b**) sliding, and (**c**) separation. The green shaded area is the friction cone. The purple shaded area is the feasible region of $\mathbf{v}$. Constraints corresponding to (8a) and (8b) are color-coded blue and red, respectively.

To show the equivalence between (9) and (10), we first write down the Lagrangian of (10):

$$
\begin{aligned}
& L\left(\boldsymbol{v}_u^{l+1}, \boldsymbol{v}_a^{l+1}, \boldsymbol{\beta}\right) \\
&= \frac{h^2}{2}\left(\boldsymbol{v}_a^{l+1}\right)^{\mathsf{T}} \boldsymbol{K}_{\boldsymbol{q}_a} \boldsymbol{v}_a^{l+1} - h\boldsymbol{\tau}_u^{\mathsf{T}} \boldsymbol{v}_u^{l+1} - h\boldsymbol{\tau}_a^{\mathsf{T}} \boldsymbol{v}_a^{l+1} \\
& -h\left(\boldsymbol{K}_{\boldsymbol{q}_a} \bar{\boldsymbol{q}}_a^l\right)^{\mathsf{T}} \boldsymbol{v}_a^{l+1} - \sum_i \sum_j \beta_{ij}\left(\frac{\phi_i^l}{h}\right. \\
& \qquad \left. + \left[\boldsymbol{n}_{i,u}^l + \mu_i \boldsymbol{d}_{ij,u}^l\right]^{\mathsf{T}} \boldsymbol{v}_u^{l+1} + \left[\boldsymbol{n}_{i,a}^l + \mu_i \boldsymbol{d}_{ij,a}^l\right]^{\mathsf{T}} \boldsymbol{v}_a^{l+1}\right)
\end{aligned} \tag{11}
$$

where $\boldsymbol{\beta} \in \mathbb{R}^{n_d}$ is the vector consisting of every β_{ij}, the Lagrange multipliers of constraint (10b).

Stationarity conditions lead to the force balance equations (9a) and (9b):

$$
\begin{aligned}
\nabla_{\boldsymbol{v}_u^{l+1}} L &= -\sum_i \sum_j \beta_{ij}\left(\boldsymbol{n}_{i,u}^l + \mu_i \boldsymbol{d}_{ij,u}^l\right) - h\boldsymbol{\tau}_u = \mathbf{0}, \\
\nabla_{\boldsymbol{v}_a^{l+1}} L &= -\sum_i \sum_j \beta_{ij}\left(\boldsymbol{n}_{i,a}^l + \mu_i \boldsymbol{d}_{ij,a}^l\right) - h\boldsymbol{\tau}_a \\
&\qquad -h\boldsymbol{K}_{\boldsymbol{q}_a}\left(\Delta\bar{\boldsymbol{q}}_a l - h\boldsymbol{v}_a^{l+1}\right) = \mathbf{0}.
\end{aligned}
$$

Complementary slackness, together with primal and dual feasibility, results in (9c).

V. Simulation Results

A. 2D Parallel Gripper

To illustrate the correctness of (10) and its "boundary layer" effect during sliding, we continue with the 2D grasping example introduced in Fig. 2 using a gripper trajectory that induces multiple contact mode changes between the fingers and the sphere. The simulation time step h is set to 0.01s; the weight of the sphere is 10N; the stiffness for all actuated DOFs is $1000\text{N}/\text{m}$ and a friction coefficient of 0.5 is used for all contacts. We will use $c_{n_i} = \lambda_{n_i}/h$ and $c_{f_i} = \lambda_{f_i}/h$ to denote the normal and tangent components of the contact forces.

As shown in Fig. 5, the grippers start 0.006m away from the surface of the sphere. They are first commanded to translate horizontally, touching the sphere at $t = 0.03$s. The grippers continue to squeeze the object until $t = 0.08$s. Accordingly, c_{n_1} grows from 0N to 10N, while ϕ_1 stays at 0. As shown in Fig. 6, this behavior is reproduced by both the LCP formulation (6) and the proposed QP (10).

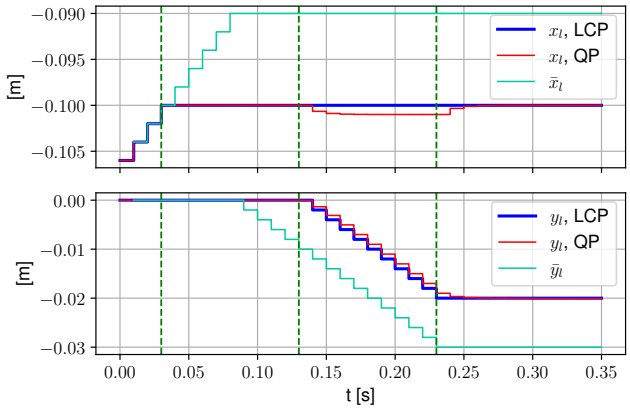

Fig. 5: Commanded and actual left finger positions, as simulated by LCP (6) and the proposed QP (10). The right finger is not shown, as the motions and forces of the left and right fingers are symmetric about the y-axis. The green dashed vertical lines indicate contact mode changes: separation to rolling at $t = 0.03$s; rolling to sliding at $t = 0.13$s; sliding to rolling at $t = 0.23$s.

The grippers are then commanded to pull downwards. Although initially resisted by friction, the downward commands eventually overcome friction and slipping starts at $t = 0.13$s. In the LCP simulation, c_{n_1}, c_{f_1} and ϕ_1 remain constant despite the contact mode transition from rolling to sliding. In the QP simulation, however, as sliding starts at $t = 0.13$s, a small increase in ϕ_1 is observed, which, as explained in Section. IV-A.2, is needed by sliding under Anitescu's friction constraints. In both the LCP and QP simulations, c_{n_3} grows with the friction c_{f_1} in order to keep the sphere in force balance.

The downward commands stop at $t = 0.24$s, and the contact mode switches back to sticking from sliding. Once again, c_{n_1}, c_{f_1} and ϕ_1 remain constant in the LCP formulation. In contrast, the "boundary layer" created by sliding in the QP formulation dissipates as sliding stops.

B. 3D pick and place

The proposed quasistatic convex time-stepping simulator is implemented in Drake [24]. Specifically, Drake's `SceneGraph` is used for collision queries, `MultibodyPlant`(MBP) for kinematics, and `MathematicalProgram` for constructing the QP (10), which is then solved with GUROBI [25]. We have found that QP (10) scales well with the number of DOFs and contacts. For the manipulation

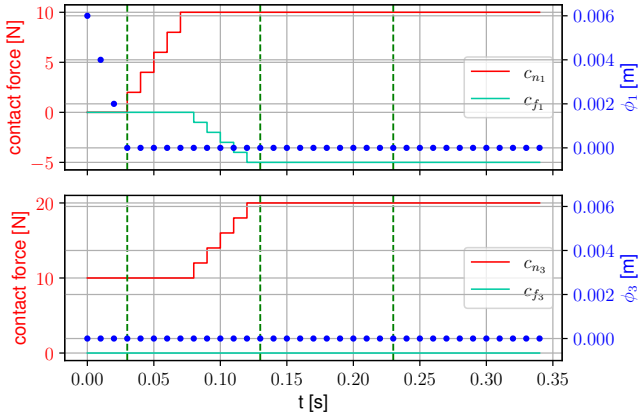

(a) Simulated by quasistatic LCP (6).

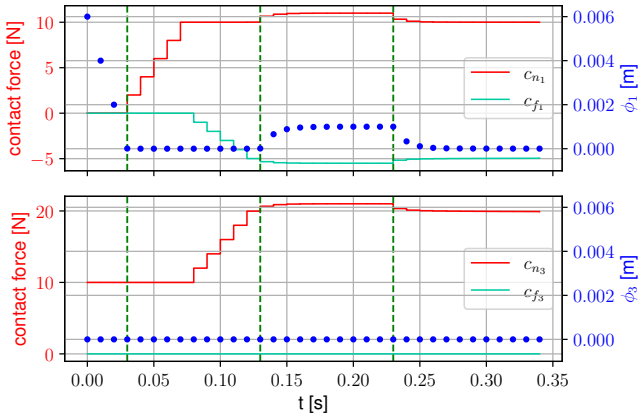

(b) Simulated by the proposed QP (10).

Fig. 6: Contact force and signed distance at contact 1 and 3 of the gripper-sphere system.

task in Fig. 1, which has 10 cubes, 69 DOFs and 56 contacts on average, the mean time of solving QP (10) is 3.56ms on a Mac mini with Intel i7-8700B CPU and 64GB of RAM.

Being able to use much larger integration time steps is a major advantage of quasistatic systems over their second-order counterparts. The quality of a simulated trajectory can be measured by its total integral error:

$$\int \|\boldsymbol{q}(t) - \boldsymbol{q}_{\text{GT}}(t)\| \, \mathrm{d}t \tag{13}$$

where $\boldsymbol{q}_{\text{GT}}(t)$ is the ground truth trajectory, which is generated with Drake's MBP using a time step $h = 5 \times 10^{-5}$s.

As shown in Fig. 7, the total integral error of MBP, a second-order simulator, starts to explode right after $h = 0.001$s. On the other hand, the total integral error of the proposed quasistatic scheme remains flat even for $h = 0.4$s.

Moreover, the increase in time step does not noticeably sacrifice fidelity. As shown in Fig. 8, the translational trajectories are almost identical to the ground truth despite the increase in h. The ground-truth angle of the cube is different by some 0.8 degrees from the angles generated by the quasistatic simulator when the cube is being lifted up (z increases) from $t = 2.5$s to 6s. We think this could be attributed to the difference in contact models used by MBP and the proposed quasistatic scheme.

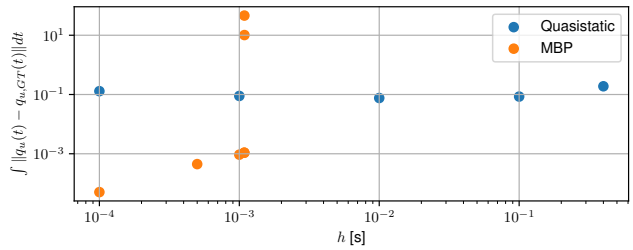

Fig. 7: Total integral error of the red cube in Fig. 1, which is picked up and placed on the stack. Trajectories of the cube are generated with MBP and the proposed quasistatic scheme using various time steps h.

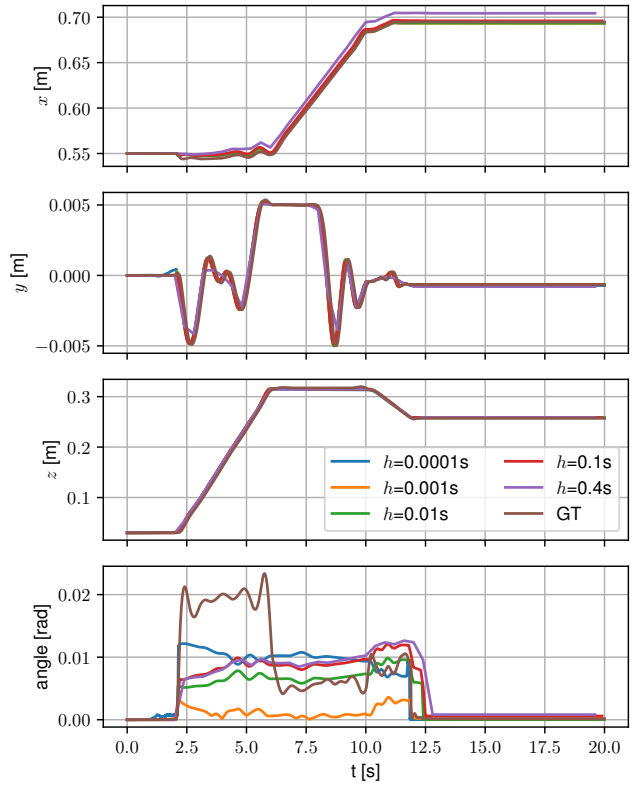

Fig. 8: Trajectories of the red cube in Fig. 1, including the ground truth (GT) and the ones generated using the proposed quasistatic scheme with different time steps h. x, y and z are the cube's center of mass coordinates in world frame. Angle comes from the axis-angle representation of the cube's orientation relative to world frame.

VI. Conclusions

We have demonstrated a convex, quasistatic time-stepping scheme that is mostly physically accurate and has good scalability. By modeling robots as impedances, the proposed scheme produces unique contact forces from commanded robot motions. The scheme also utilizes a relaxed friction constraints which can be formulated as the KKT condition of a convex QP. The friction constraints add a thin boundary layer between relatively-sliding objects, but are otherwise equivalent to Coulomb's friction law. The proposed quasistatic simplifications allow significantly larger simulation time steps without sacrificing accuracy, which can be capitalized to considerably speed up the simulation of robotic manipulation tasks.

REFERENCES

[1] M. Anitescu and F. A. Potra, "Formulating dynamic multi-rigid-body contact problems with friction as solvable linear complementarity problems," *Nonlinear Dynamics*, vol. 14, no. 3, pp. 231–247, 1997.

[2] D. E. Stewart, "Rigid-body dynamics with friction and impact," *SIAM review*, vol. 42, no. 1, pp. 3–39, 2000.

[3] R. W. Cottle, J.-S. Pang, and R. E. Stone, *The linear complementarity problem*. SIAM, 2009.

[4] M. Anitescu, "Optimization-based simulation of nonsmooth rigid multibody dynamics," *Mathematical Programming*, vol. 105, no. 1, pp. 113–143, 2006.

[5] E. Todorov, "Convex and analytically-invertible dynamics with contacts and constraints: Theory and implementation in mujoco," in *2014 IEEE International Conference on Robotics and Automation (ICRA)*. IEEE, 2014, pp. 6054–6061.

[6] E. Drumwright and D. A. Shell, "Modeling contact friction and joint friction in dynamic robotic simulation using the principle of maximum dissipation," in *Algorithmic foundations of robotics IX*. Springer, 2010, pp. 249–266.

[7] G. Brockman, V. Cheung, L. Pettersson, J. Schneider, J. Schulman, J. Tang, and W. Zaremba, "Openai gym," *arXiv preprint arXiv:1606.01540*, 2016.

[8] M. T. Mason, "Mechanics and planning of manipulator pushing operations," *The International Journal of Robotics Research*, vol. 5, no. 3, pp. 53–71, 1986.

[9] K. M. Lynch and M. T. Mason, "Stable pushing: Mechanics, controllability, and planning," *The International Journal of Robotics Research*, vol. 15, no. 6, pp. 533–556, 1996.

[10] F. R. Hogan and A. Rodriguez, "Feedback control of the pusher-slider system: A story of hybrid and underactuated contact dynamics," *arXiv preprint arXiv:1611.08268*, 2016.

[11] J. Zhou, J. A. Bagnell, and M. T. Mason, "A fast stochastic contact model for planar pushing and grasping: Theory and experimental validation," in *Robotics: Science and systems XIII*, 2017.

[12] J. C. Trinkle, R. Ram, A. Farahat, and P. F. Stiller, "Dexterous manipulation planning and execution of an enveloped slippery workpiece," in *[1993] Proceedings IEEE International Conference on Robotics and Automation*. IEEE, 1993, pp. 442–448.

[13] J.-S. Pang, J. C. Trinkle, and G. Lo, "A complementarity approach to a quasistatic multi-rigid-body contact problem," *Computational Optimization and Applications*, vol. 5, no. 2, pp. 139–154, 1996.

[14] T. Pang and R. Tedrake, "A robust time-stepping scheme for quasistatic rigid multibody systems," in *2018 IEEE/RSJ International Conference on Intelligent Robots and Systems (IROS)*. IEEE, 2018, pp. 5640–5647.

[15] M. Halm and M. Posa, "A quasi-static model and simulation approach for pushing, grasping, and jamming," in *International Workshop on the Algorithmic Foundations of Robotics*. Springer, 2018, pp. 491–507.

[16] R. Tedrake, "Underactuated robotics: Algorithms for walking, running, swimming, flying, and manipulation (course notes for mit 6.832)." [Online]. Available: http://underactuated.mit.edu/

[17] R. Kolbert, N. Chavan-Dafle, and A. Rodriguez, "Experimental validation of contact dynamics for in-hand manipulation," in *International Symposium on Experimental Robotics*. Springer, 2016, pp. 633–645.

[18] S. Goyal, A. Ruina, and J. Papadopoulos, "Planar sliding with dry friction part 1. limit surface and moment function," *Wear*, vol. 143, no. 2, pp. 307–330, 1991.

[19] R. D. Howe and M. R. Cutkosky, "Practical force-motion models for sliding manipulation," *The International Journal of Robotics Research*, vol. 15, no. 6, pp. 557–572, 1996.

[20] J. Trinkle, S. Berard, and J. Pang, "A time-stepping scheme for quasistatic multibody systems," in *Assembly and Task Planning: From Nano to Macro Assembly and Manufacturing, 2005.(ISATP 2005). The 6th IEEE International Symposium on*. IEEE, 2005, pp. 174–181.

[21] D. Prattichizzo and J. Trinkle, *Springer Handbook of Robotics*. Springer Handbooks. Springer, Cham., 2016, ch. Grasping.

[22] N. Hogan, "Impedance control: An approach to manipulation: Part i—theory," 1985.

[23] C. Ott, A. Albu-Schaffer, A. Kugi, and G. Hirzinger, "On the passivity-based impedance control of flexible joint robots," *IEEE Transactions on Robotics*, vol. 24, no. 2, pp. 416–429, 2008.

[24] R. Tedrake and the Drake Development Team, "Drake: A planning, control, and analysis toolbox for nonlinear dynamical systems," 2020. [Online]. Available: http://drake.mit.edu

[25] Gurobi Optimization, Inc., "Gurobi optimizer reference manual," 2017. [Online]. Available: http://www.gurobi.com/